SF2A 2023
M. N'Diaye, A. Siebert, N. Lagarde, O. Venot, K. Baillié, M. Béthermin, E. Lagadec, J. Malzac, J. Richard (eds)

A MAGNETIC FIELD STUDY IN THE ENVELOPE OF COOL EVOLVED STARS

L. Marinho[1], F. Herpin[1], H. Wiesemeyer[2], A. López-Ariste[3], A. Baudry[1], A. Asensio Ramos[4] and the PEPPER team

Abstract. Evolved cool stars exhibit a massive mass loss, which contributes to the enrichment of the interstellar medium and therefore to the recycling of matter in the Universe. The mechanisms (e.g. the stellar magnetic field) behind this mass loss phenomena are not understood, but can be constrained thanks to observations of the star and its circumstellar envelope (CSE). Here, we focus on the SiO maser line emission, which probes the inner region of the envelope (2-4 stellar radii from the photosphere) and can reveal the presence of a magnetic field. With radio-astronomical polarimetric observations, we derive the angle of polarization, the linear and circular polarization, which according to theories can lead to an estimate of the magnetic field strength along the line of sight. The magnetic field strength is hence estimated at between 0.1 and 10 G. A global poloidal field can be excluded. There are still questions about the origin of the magnetic field (solar-type dynamo, turbulent dynamo ...) and its evolution.

Keywords: masers – polarization – stars: evolution, late-type, magnetic field

1 Introduction

Over 95% of the stars in the Galaxy are low- or intermediate-mass star (under $8M_{\odot}$; Salpeter (1955); Chabrier (2003)). After the Main Sequence, these stars will evolve through different stages, including the Asymptotic Giant Branch (AGB) phase. During the few million years they will spend on the AGB, their circumstellar envelope (CSE) will become an impressive chemical factory, where more than 80 molecules and 15 dust species have been discovered (Höfner & Olofsson 2018; Decin et al. 2018). The important mass loss that these stars experience ($10^{-4} - 10^{-6}$ $M_{\odot}$/yr, Höfner & Olofsson 2018; Decin et al. 2018) makes them important actors in the recycling in the Universe, contributing at 85% to the gas enrichment of all stellar sources and at 35% of the total enrichment of the ISM. What triggers and shapes those strong winds is still debated and not fully understood. The magnetic field is expected to be a potential agent in the mass loss process (Pascoli & Lahoche 2008) and in shaping the wind. It has already been detected in the CSE through observations of different maser lines, probing the magnetic field at different distances from the star: SiO in the inner region of the CSE (Herpin et al. 2006), OH and H_2O in the more outer regions (Rudnitski et al. 2010). Optical spectropolarimeters (ESPaDOnS@CFHT, Narval@TBL) have contributed a lot of information on the magnetic activity on the stellar surface.

2 Observations

We observed the SiO v=1, J=2-1 maser line at 86.2434277 GHz with the IRAM-30m telescope in March and May 2022. Our sample is made of 6 evolved stars: 5 Mira-type AGB (χ Cyg, o Ceti, R Aql, R Leo and U Her) and one RSG (Red super giant) μ Cep, described in Table 1. We obtained the Stokes parameters with instrument XPol (Thum et al. 2008), using the EMIR receiver (E90 frontend band), and VESPA backend.

We verified the polarization angle calibration with the Crab Nebula, a well-known, strongly linearly polarized source. The instrumental polarization on the optical axis was verified on a planet (Uranus) as a non-polarized

[1] Laboratoire d'astrophysique de Bordeaux, Univ. Bordeaux, CNRS, B18N, allée Geoffroy Saint-Hilaire, 33615 Pessac, France.
[2] Max-Planck-Institut für Radioastronomie, Auf dem Hüugel 69, 53121 Bonn, Germany
[3] IRAP, Université de Toulouse, CNRS, CNES, UPS, 14 Av. E. Belin, 31400 Toulouse, France,
[4] Instituto de Astrofísica de Canarias, La Laguna

Star	RA (J2000) [h m s]	DEC (J2000) [° ’ ”]	Type	d [pc]	L [$L_\odot$]	T_{eff} [K]	Mass-Loss rate [$M_\odot$/yr]
o Ceti[a]	02:19:20.79	-02:58:39.50	Mira	107	6099	2193	2.5×10^{-7}
R Leo[b]	09:47:33.49	+11:25:43.82	Mira	100	5617	2890	9.2×10^{-7}
U Her[b,c]	16:25:47.47	18:53:32.86	Mira	271	8000	3000	5.9×10^{-7}
R Aql[b,c]	19:06:22.25	08:13:48.01	Mira	308	4900	2800	1.1×10^{-6}
χ Cyg[b]	19:50:33.92	+32:54:50.61	Mira	180	7813	2000	2.4×10^{-7}
μ Cep[d,e]	21:43:30.46	+58:46:48.16	RSG	390/1818	35000	3750	2.0×10^{-6}

Table 1. List of the observed sources, data from [a]De Beck et al. (2010), [b] Andriantsaralaza et al. (2022), [c]Gottlieb et al. (2022), [d]Montargès et al. (2019), [e]Maercker et al. (2022)

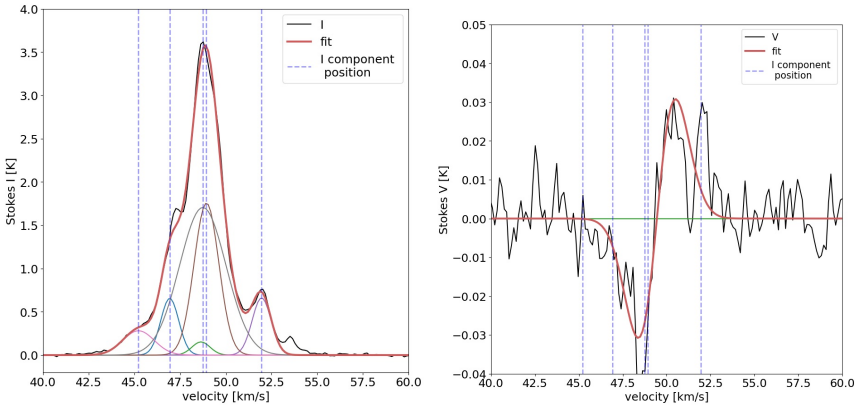

Fig. 1. Decomposition by the *rvm* code. **Left:** Stokes I decomposition, the data are in black and the fit in red is the sum of all the Gaussian components (in color). The dashed purple vertical lines are the position of the central velocity of the Gaussian functions. **Right:** Stokes V decomposition with the same color as before.

source. From the Stokes parameters I, Q, V and U we can compute the circular polarization rate ($p_{\rm C}$), the linear polarization rate ($p_{\rm L}$), and the angle of polarization (χ). The instrumental and astronomical contributions to the linear polarization were separated thanks to the modulation of the former in the celestial reference frame. For the circular polarization, we developed a method to remove the instrumental contamination from the data.

3 Data analysis and method

3.1 Stokes I and V decomposition

For an analysis based on the Zeeman theory, we first decomposed Stokes I into a combination of Gaussian functions.

$$I(v) = \sum_{k=1}^{n} A_k e^{-\frac{(v-v_{0,k})^2}{\Delta v_{D,k}^2}} \tag{3.1}$$

with $v_{0,k}$ and $v_{D,k}$ respectively the central velocity and Doppler width for each component k, and A_k a weight. We develop a code based on the relevant vector machine (Tipping & Faul 2003). The *rvm* code finds the best linear combination of entries from a dictionary. In our case, it will find the best number of Gaussians from a dictionary of parameters that we fixed. The dictionary is made of 200x50 parameters, with 200 central velocities and 50 line-width ranges. We can do the same for Stokes V. Based on the Zeeman theory, V can be written as $V(\lambda) = f(B)\frac{dI}{d\lambda}$ with $f(B)$ a function of the magnetic field. An example of decomposition of Stokes V in a sum of the derivative of Gaussian functions is shown in Figure 1.

3.2 Magnetic field estimate

We compute the magnetic field strength at the two V peaks of each Zeeman component found by the code: $\lambda_{peak} = \lambda_0 \pm \frac{1}{\sqrt{2}}\Delta\lambda_{\rm D}$. This calculation depends on the saturation level of the maser emission. To estimate

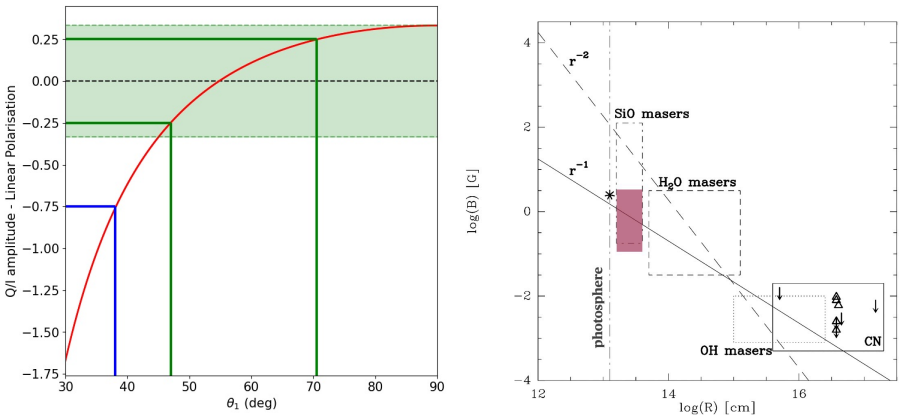

Fig. 2. Left: Linear polarization vs the angle for B=1G. The blue solution represents a case where $|q| > q_c$, the green one where $|q| < q_c$. The green-shaded area indicates the loci where two solutions exist. **Right:** The magnetic field strength as a function of the distance. The dotted squares are previous observations (Herpin et al. 2006; Rudnitski et al. 2010; Duthu et al. 2017) and the red one is the new results computed here, constraining the magnetic field in r^{-1}.

this saturation level, we compute the stimulated emission rate $R = \frac{AkT_b\Delta\Omega}{4\pi h\nu}$, with A the Einstein coefficient for spontaneous emission of the transition, k the Boltzmann constant, T_b the brightness temperature, and $\Delta\Omega$ the solid beaming angle (the ratio of the surface area of the maser spot area to that of the masing cloud). This parameter is not well known and we adopt a minimal value: 5×10^{-2} from Assaf et al. (2013). Considering R and the linear polarization fraction(Nedoluha & Watson 1990), we consider two strongly saturated sources (χ Cyg and U Her), two not strongly saturated (R Aql and μ Cep), and two sources where we can't conclude (o Ceti and R Leo.)

We thus consider two cases:

$$\textbf{Saturated maser (Elitzur 1996):}\quad \frac{B}{\cos\theta_1} \simeq 65\Delta v_{\rm D}\frac{V(v_{peak})}{I(v_{peak})} \tag{3.2}$$

$$\textbf{Unsaturated maser (Zeeman weak field theory):}\quad B\cos\theta_2 \simeq 33.73\frac{V(v_{peak})}{\partial_v I(v_{peak})} \tag{3.3}$$

B is in Gauss and $\Delta v_{\rm D}$ is the width of the Gaussian used in the *rvm* code to fit the Stokes V. In Both formula, there is still a dependence on the angle (θ_1 is the angle between $\vec{B}$ and the incident beam, θ_2 is the angle between $\vec{B}$ and the refracted beam). We can't derive the angle from the Zeeman weak field theory, but we can for the strongly saturated maser. Following Elitzur (1996), in a coordinate system that is aligned with the sky-plane projected magnetic field, $q = Q/I$ is given by: $q = 1 - 2\frac{3-R_1}{(2R_1+1)\sin^2\theta_1}$ with $R_1 = 1 - x_B^2(1-2\lambda^2)$ and x_B the ratio of the Zeeman splitting Δv_B to the Doppler line-width $\Delta v_{\rm D}$. So $R_1 = 1 - 14^2 g^2 \lambda_0^2 B^2 (1-2\lambda^2)/\Delta\lambda_D^2$ where g is the Landé factor, λ_0 the wavelength of the maser emission, and B the magnetic field strength in Gauss. This equation is plotted in Figure 2, left. As we only have the absolute value of $p_{\rm L}$ in the observations, depending on the values of $p_{\rm L}$, we have two possibilities. There is a critical value q_c defined by $\lim_{\theta\to+90^\circ} q = 0.333$. If $|q| > q_c$: the solution for the angle θ_2 is unique (see example in blue in the Figure 2, left). And if $|q| < q_c$, there are two solutions for θ_2 (see the example in green), and hence two solutions for the magnetic field strength.

Uncertainties computation: There are two main sources of uncertainties. 1/ A remaining instrumental polarization in the data that we quantified, $\delta V_{\rm inst} = 7$ mK for the sample. 2/ The difference between the fit and the observational data ($\delta V_{\rm noise}$).

4 Results and Discussion

Applying this, we compute the magnetic field for all the sources (see Fig. 3) and the results were added in red in Figure 2 right. The magnetic field seems to evolve in r^{-1} in agreement with the point on the photosphere, measured for χ Cyg (Lèbre et al. 2014). We also have two periods of observation for U Her, and we can see that the magnetic field has changed in two months. So far we have no stringent explanation for this change,

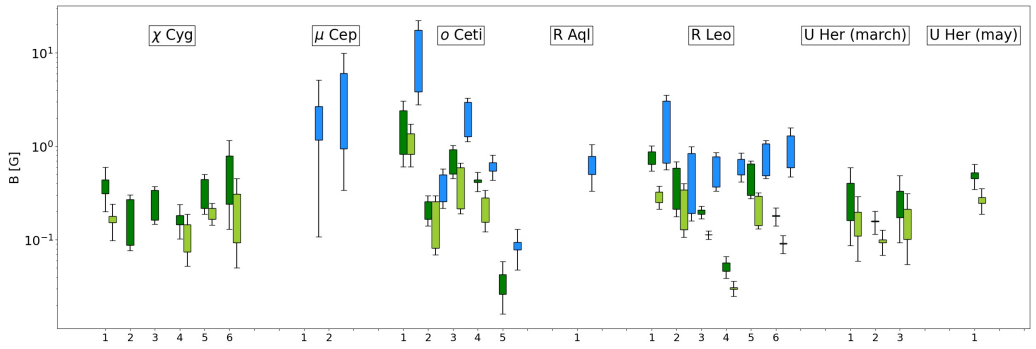

Fig. 3. Magnetic field strength for all sources, depending on the Gaussian component as indicated on the x-axis. The blue results are for mildly strongly saturated maser, the green ones are the strongly saturated solution. Two green bars for the same Gaussian component indicate that p_L is under 33%, entailing two magnetic-field solutions. For μ Cep and R Leo, the strongly saturated and the not strongly saturated solution are shown.

but it is probably correlated with the stellar activity and the presence of cool spots on the stellar surface (Soker 2002). A turbulent dynamo mechanism ($\alpha^2 - \omega$) can generate a weak magnetic field at the stellar surface, that is amplified by shocks and convection above the cool spots.

5 Conclusions

We developed a method to estimate the magnetic field in the inner region of the envelope of cool evolved stars. We were able to remove the instrumental contamination. We found a magnetic field between 0.1 and 10 Gauss. This result suggests that the magnetic field evolves in r^{-1} in the envelope. There is still work to be done to understand the temporal evolution and the origin of the magnetic field.

Acknowledgements: This work is funded by the French National Research Agency (ANR) project PEPPER (ANR-20-CE31- 0002)

References

Andriantsaralaza, M., Ramstedt, S., Vlemmings, W. H. T., & De Beck, E. 2022, A&A, 667, A74
Assaf, K. A., Diamond, P. J., Richards, A. M. S., & Gray, M. D. 2013, Monthly Notices of the Royal Astronomical Society, 431, 1077
Chabrier, G. 2003, PASP, 115, 763
De Beck, E., Decin, L., de Koter, A., et al. 2010, A&A, 523, A18
Decin, L., Richards, A. M. S., Danilovich, T., Homan, W., & Nuth, J. A. 2018, A&A, 615, A28
Duthu, A., Herpin, F., Wiesemeyer, H., et al. 2017, A&A, 604, A12
Elitzur, M. 1996, The Astrophysical Journal, 457, 415
Gottlieb, C. A., Decin, L., Richards, A. M. S., et al. 2022, A&A, 660, A94
Herpin, F., Baudry, A., Thum, C., Morris, D., & Wiesemeyer, H. 2006, A&A, 450, 667
Höfner, S. & Olofsson, H. 2018, A&A Rev., 26, 1
Lèbre, A., Aurière, M., Fabas, N., et al. 2014, A&A, 561, A85
Maercker, M., Khouri, T., Mecina, M., & De Beck, E. 2022, A&A, 663, A64
Montargès, M., Homan, W., Keller, D., et al. 2019, MNRAS, 485, 2417
Nedoluha, G. E. & Watson, W. D. 1990, ApJ, 354, 660
Pascoli, G. & Lahoche, L. 2008, PASP, 120, 1267
Rudnitski, G. M., Pashchenko, M. I., & Colom, P. 2010, Astronomy Reports, 54, 400
Salpeter, E. E. 1955, ApJ, 121, 161
Soker, N. 2002, MNRAS, 336, 826
Thum, C., Wiesemeyer, H., Paubert, G., Navarro, S., & Morris, D. 2008, PASP, 120, 777
Tipping, M. E. & Faul, A. C. 2003, in Proceedings of Machine Learning Research, Vol. R4, Proceedings of the Ninth International Workshop on Artificial Intelligence and Statistics, ed. C. M. Bishop & B. J. Frey (PMLR), 276–283, reissued by PMLR on 01 April 2021.